01 Mar 2001

# Network Formalism for Modeling Functionally Gradient Piezoelectric Plates and Stacks and Simulations of RAINBOW Ceramic Actuators

Robert W. Schwartz
*Missouri University of Science and Technology*

A. Ballato

John Ballato



## Recommended Citation

R. W. Schwartz et al., "Network Formalism for Modeling Functionally Gradient Piezoelectric Plates and Stacks and Simulations of RAINBOW Ceramic Actuators," *IEEE Transactions on Ultrasonics, Ferroelectrics and Frequency Control*, Institute of Electrical and Electronics Engineers (IEEE), Mar 2001.
The definitive version is available at https://doi.org/10.1109/58.911729

# Network Formalism for Modeling Functionally Gradient Piezoelectric Plates and Stacks and Simulations of RAINBOW Ceramic Actuators

John Ballato, *Member, IEEE*, Robert Schwartz, *Member, IEEE*, and Arthur Ballato, *Fellow, IEEE*

***Abstract*—A simple network representation is given for a stack of thin, homogeneous piezoelectric plates, executing a single thickness mode of motion. All plates may differ in thickness and material properties, including dielectric loss, ohmic conductivity, and viscous loss. Each plate is driven by a thickness-directed electric field, and all stack elements are connected electrically in series. Functionally gradient single plates and composites are readily modeled by the network, to a desired precision, using a sequence of circuit elements representing stepwise variations in material properties and layer thicknesses. Simulations of RAINBOW (Reduced And Internally Biased Oxide Wafer) ceramics are given.**

## I. Introduction

Materials deliberately fashioned to have spatially varying characteristics are designated as "functionally gradient." These range from nanoscale modulation-doped semiconductors [1] to macroscopic RAINBOW ceramics [2], [3] and various other devices, configurations, and systems [4]–[11]. Spatial distributions in parameters (e.g., elastic, thermoelastic, piezoelectric, and dielectric material properties), result in unique operational attributes, but make characterization and modeling more difficult. Many of the devices in this category are piezoelectrics used for sensing and actuation, such as micro-electro-mechanical structures (MEMS). For these electromechanical systems, characterization usually takes the form of an equivalent network because the device itself forms part of the overall circuitry.

Equivalent electrical networks have been utilized successfully for many years to model the behavior of both individual and cascaded piezoelectric resonator and transducer structures. Lumped-element circuits of the Butterworth-Van Dyke (BVD) type [12]–[14] are apt for simulating resonator and transducer behavior in a narrow frequency band centered about a single harmonic. Distributed (acoustic transmission line) equivalent networks are suited to wideband operation and fall into two main categories: Mason-type circuits, [15]–[20] and those of Krimholtz, Leedom, and Matthaei (KLM) [19], [21]–[23]. These network embodiments both realize exactly the three-port immittance relations derived from the physics of the situation but are distinguished by internal topology and circuit components. Transmission-line (TL) circuits of the Mason type have been derived for homogeneous piezoelectrics, and attempts have been made to apply them to the case of spatially nonuniform piezoelectric constants [24]. The KLM networks, in their current form, permit modeling of layers with arbitrary piezoelectric gradients but require unvarying elastic properties and the evaluation of Hilbert and Fourier transforms. Further, the incorporation of losses into KLM-type circuits has not been explored. In the vicinity of a single resonance, Mason-type circuits are often reduced to a lumped representation, either of the simple BVD variety or extensions thereof [25], for which the effects of loss mechanisms are manifested by the presence of one or more resistors.

We furnish here a network realization, of relatively simple form, of a practical and widely occurring electromechanical implementation: a one-dimensional stack of piezoelectric plates driven by thickness excitation (TE). It is based on a cascade of circuits of the Mason type, but provision is also made for inclusion of three separate types of material loss mechanisms in each plate: viscous and dielectric loss and ohmic conductivity. The network model is applied to the characterization of functionally gradient structures by matching the parameters of the individual TL circuits to the local environment of the material at each increment of the thickness coordinate. As the number of TLs grows, their individual sizes diminish, and the overall network approximates a continuous distribution of material parameters [26].

Although the number of discrete plates that can be accommodated by the network model is not limited, when applied to many practical implementations of functional grading, the number of circuits in the cascade required to yield good modeling accuracy can be surprisingly few. Explicit forms of the overall electromechanical network impedance matrix are given for stacks consisting of one to six layers, from which the rule of formation for the general case is obtained.

As examples, the formalism is applied to two types of simulations. In the first, a ceramic/cermet composite resonator is simulated both as a two-layer asymmetric stack and as a single ceramic plate with asymmetric lumped surface mass representing the effect of the cermet. Results are given for a variety of ceramic/cermet ratios. In the

Manuscript received October 5, 1999; accepted July 19, 2000. J. Ballato and R. Schwartz acknowledge NASA (contract # NCC1-283) for partial support of this work.

J. Ballato and R. Schwartz are with the Department of Ceramic and Materials Engineering, Clemson University, Clemson, SC 29634-0907 (e-mail: john.ballato@ces.clemson.edu).

A. Ballato is with US Army Communications-Electronics Command, AMSEL-RD-CS, Fort Monmouth, NJ 07703-5201.

second set of simulations, a linear spatial gradation in material properties, from pure ceramic to pure cermet, is approximated using a sequence of stacks of varying numbers. These structures are representative of RAINBOW ceramic transducers. For all cases, lists of symbols used, with units and dimensions, are provided in Appendix A.

## II. Single Plate Resonator [27]

We assume only one acoustic thickness mode of vibration. This is the case for a thin piezoelectric plate of symmetry class 6 mm, such as a piezoceramic, excited by TE along the thickness-directed polar axis. This mode is the familiar thickness-stretch mode (also called thickness extension). The piezoelectric constant is $e_{33}$, and the piezoelectrically stiffened elastic constant is $\bar{c} = c_{33}^{E} + e_{33}^{2}/\varepsilon_{33}$. If the polar axis is in the plane of the plate instead, the mode driven by TE is thickness shear, via the $e_{15}$ constant. Displacement is still along the polar axis, and the effective elastic stiffness for this mode is $\bar{c} = c_{44}^{E} + e_{15}^{2}/\varepsilon_{11}$. The subsequent analysis applies rigorously to either of these ideal cases, and approximately to many practical embodiments, as long as one is dealing with a substantially laterally invariant single mode, well separated in frequency from other resonances, and uses the appropriate numerical values. These assumptions allow a one-dimensional treatment to be used. If the polarization is not strictly along the thickness, and/or the driving field is not strictly in the thickness direction, then the situation is somewhat more complicated [28] and is not covered here although the approach described here would apply.

### *A. The Plate Impedance Matrix*

A three-port electromechanical network, N, representing the plate is shown in Fig. 1. Because the plate is TE driven, it is simplest to characterize it by an impedance matrix [17]. Port 1 is the 'left' surface; Port 2 is the 'right' surface; and Port 3 is the electrical port, consisting of the connections to the two outer electrodes. Variables at Port 3 are electrical voltage and current; those at mechanical Ports 1 and 2 are, correspondingly, force (surface stress times electrode area) and particle velocity (angular frequency times particle displacement for time-harmonic motion). Subscripts on immittance relations refer by number to these ports.

The following definitions hold throughout the rest of the paper: electrode area, A; plate thickness, $t = 2h$; piezoelectrically stiffened acoustic velocity, v; acoustic impedance, $Z_o = A \cdot \rho \cdot v$; static capacitance, $C_o = \varepsilon \cdot A/t$; piezoelectrically stiffened elastic stiffness, $\bar{c} = \rho \cdot v^2$; piezocoupling coefficient, $k = e/\sqrt{\varepsilon \bar{c}}$; piezoelectric transformer turns ratio, $n = A \cdot e/t$; angular frequency, $\omega = 2\pi f$, where f is the frequency variable; fundamental mechanical frequency, $f_o = v/2t$; normalized frequency variable, $X = (\pi/2) \cdot (f/f_o)$; and mechanical loads at Ports 1 and 2, $Z_L$ and $Z_R$, respectively.

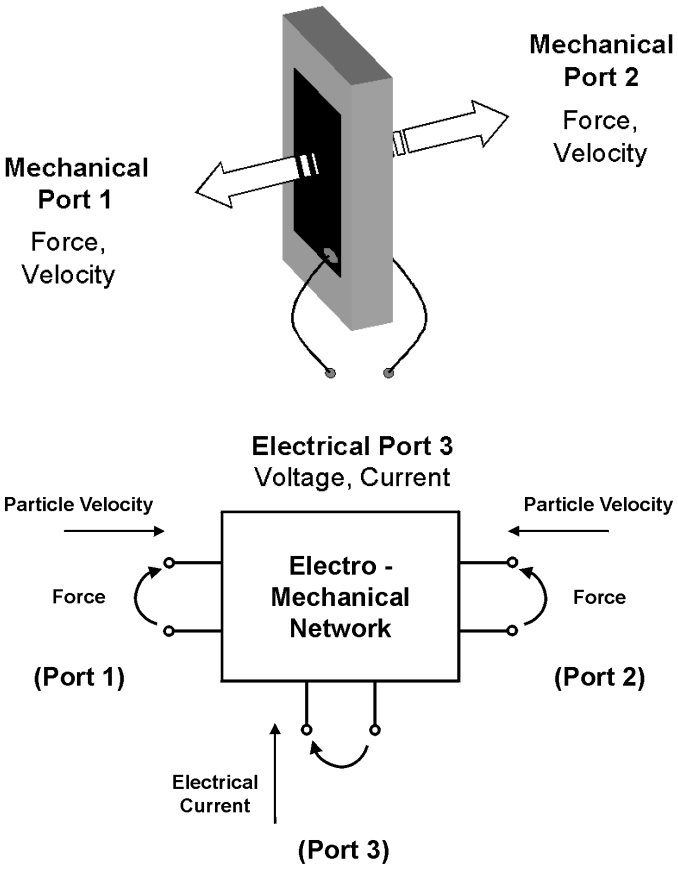


Fig. 1. Piezoelectric plate resonator and its three-port electromechanical network representation. a) Electroded plate resonator. Ports 1 and 2 are the major surfaces characterized by force and particle velocity as analogs to electrical voltage and current; Port 3 is the electrical attachment to the electrodes. b) Schematic representation of the three-port electromechanical network.

Elements of the lossless symmetric impedance matrix,[1] $[z^0]$, of network N are as follows [19]: $z_{11} = z_{22} = Z_o/[j \cdot \tan(2X)]$; $z_{12} = Z_o/[j \cdot \sin(2X)]$; $z_{13} = z_{23} = n/[j\ \omega\ C_o]$; and $z_{33} = 1/[j\ \omega\ C_o]$. Elements of the symmetric mechanical load impedance matrix, $[z_{LOAD}]$, are defined as follows: $z_{11LOAD} = Z_L; z_{22LOAD} = Z_R; z_{33LOAD} = z_{12LOAD} = z_{13LOAD} = z_{23LOAD} = 0$. The total impedance matrix, [z], is the sum of these two matrices, and its reciprocal is the admittance matrix, [y], of the piezoresonator with mechanical loads at Ports 1 and 2. All elements of the piezoelectric impedance matrix are functions of frequency; this will usually also be true for the mechanical load matrix elements $Z_L$ and $Z_R$. Material loss mechanisms within the plate have not yet been introduced, yet [y] will, in general, still be complex because $Z_L$ and $Z_R$ may have resistive components caused by energy transport and/or dissipation.

[1]Impedance and admittance matrices, [z] and [y], respectively, written with superscripts (e.g., $[z^0]$) are not to be construed as exponents.

### B. Mechanical Surface Loadings

When the resonator surface is mechanically loaded only by electrode masses, $Z_L$ and $Z_R$ are purely reactive and represent inertial effects. The lumped electrode masses are represented in normalized form by the quantities $\mu_L$ and $\mu_R$. These electrode masses are equal to the areal mass ($m_e = \rho_e\, t_e$) divided by the mass per unit area of a piezoelectric plate of half-thickness, ($\rho\, h$). The acoustic loads are given in this case by the lossless relations: $Z_L = j\,\mu_L\, Z_o\, X = A \cdot j\,\omega\, m_{eL}$ and $Z_R = j\,\mu_R\, Z_o\, X = A \cdot j\,\omega\, m_{eR}$.

As an important aside, when electrode loading is negligible but the resonator is immersed in a fluid, one must distinguish among the modes of vibration executed by the piezoresonator. If the resonator vibrates in an extensional mode, the fluid loading is represented, to a very good approximation, by a purely resistive, and generally dispersionless impedance: $Z_L = Z_R = A \cdot \rho_{fluid} \cdot v_{fluid}$. This resistance is due to the transport of acoustic energy outward from the active surfaces of the plate. If the vibrational mode is shear, the Newtonian shear viscosity of the fluid produces a combination of viscous and inertial effects. The viscous part is due to the lossy drag of the evanescent shear 'wave' in the fluid; the inertial portion arises from fluid entrainment. The complex load impedance is $Z_L = Z_R = A \cdot \sqrt{(j \cdot \omega \cdot \rho_{fluid} \cdot \eta_{fluid})} = A \cdot (1+j) \cdot \sqrt{(\omega \cdot \rho_{fluid} \cdot \eta_{fluid}/2)}$. These relations permit the methodology developed here to be applied to the characterization of piezoelectric sensors subjected to fluid loadings. Accordingly, the network representations presented here are equally useful to simulate and model fluid pumps and sensors based on technologies utilizing functionally gradient structures. [29]

### C. Inclusion of Material Losses

One includes the effects of loss within the material differently, depending on the loss mechanism. Viscous loss, resulting from various acoustic scattering mechanisms, for example, is incorporated by adding an imaginary component to the acoustic stiffness: $c^* = \bar{c} \cdot (1 + j\,\omega\,\eta)$. Dielectric losses are modeled by making the permittivity complex: $\varepsilon^* = \varepsilon'(\omega) - j\varepsilon''(\omega)$; if negligible compared with other losses, $\varepsilon^*$ reduces to $\varepsilon'$, a purely real quantity. These substitutions render v, $Z_o$, X, $C_o$, and k complex. With the presence of only elastic and dielectric losses, $[z^o]$ is written as $[z^1]$, and $[y] = [z]^{-1} = \{[z^1] + [z_{LOAD}]\}^{-1}$.

Ohmic conductivity, $\sigma$, is incorporated differently from dielectric loss and appears as a shunt conductance, $G_o = \sigma \cdot A/t$, across the electrical port. When ohmic conductivity is present, [y] is obtained as follows: $[y] = [z]^{-1} = \{[z^2] + [z_{LOAD}]\}^{-1}$, where $[z^2] = \{[z^1]^{-1} + [G]\}^{-1}$ and [G] consists of null elements, except for $G_{33} = G_o$.

### D. Network Functions

The symmetric $3 \times 3$ admittance matrix, [y], describes the behavior with frequency of the boundary-loaded, lossy, single-plate resonator. Because it is driven by an excitation voltage at electrical Port 3, matrix elements $y_{q3}$, ($q = 1, 2, 3$) are pertinent. The array elements $y_{13}$ and $y_{23}$ give the particle velocities, per volt applied, at surfaces 1 and 2, respectively. Division of these by $\omega$ yields the surface displacements, $U_L$ and $U_R$, which, in general, will be complex numbers that represent motions in phase and in time quadrature with the applied voltage. Element $y_{33}$ is the input electrical admittance observed looking into Port 3; its real and imaginary parts are the input conductance and susceptance.

## III. The Two-Layer Stack

It is assumed that both plates have common electrode area, A. If shear motion is considered, then it is further assumed that the polar axes of both plates are parallel. The network representation of a two-layer stack is shown in Fig. 2. The structure has mechanical surface loadings on the outer surfaces and is driven in TE with excitation voltage impressed across the total thickness, resulting in a common electrical current. The mechanical surface loadings may be lumped electrode masses or represent additional plates.

Each plate of the stack is represented by a network $N_L$, $N_R$ whose lossy $3 \times 3$ impedance matrix is formed as discussed in the last section, giving $[z^2]_L$ and $[z^2]_R$. In this paper, the elements of $[z^2]$ will be written, henceforth, with the superscript '2' dropped. The explicit impedance relations, including symmetries, for both plates are

$$\begin{bmatrix} V_{1L} \\ V_{2L} \\ V_{3L} \end{bmatrix} = \begin{bmatrix} z_{11L} & z_{12L} & z_{13L} \\ z_{12L} & z_{11L} & z_{13L} \\ z_{13L} & z_{13L} & z_{33L} \end{bmatrix} \begin{bmatrix} I_{1L} \\ I_{2L} \\ I_{3L} \end{bmatrix}$$

$$\begin{bmatrix} V_{1R} \\ V_{2R} \\ V_{3R} \end{bmatrix} = \begin{bmatrix} z_{11R} & z_{12R} & z_{13R} \\ z_{12R} & z_{11R} & z_{13R} \\ z_{13R} & z_{13R} & z_{33R} \end{bmatrix} \begin{bmatrix} I_{1R} \\ I_{2R} \\ I_{3R} \end{bmatrix}.$$

Port 1 of $N_L$ is connected on its left to mechanical impedance $Z_L$; Port 2 of $N_L$ is joined to Port 1 of $N_R$. Port 2 of $N_R$ is connected on its right to mechanical impedance $Z_R$. The electrical Ports 3 are connected in series and have total voltage V impressed. Boundary conditions for the stack are therefore given as follows:

- outer mechanical ports: $V_{1L} = -Z_L\, I_{1L}$ and $V_{2R} = -Z_R\, I_{2R}$
- junction of $N_L$ and $N_R$: $V_{2L} = V_{1R} = V_A$ and $I_{2L} = -I_{1R} = I_A$
- electrical ports: $I_{3L} = I_{3R} = I$ and $V_{3L} + V_{3R} = V$

where $I_{1L} = I_L$; $I_{2R} = I_R$; $\zeta_{11L} = (z_{11L} + Z_L)$, and $\zeta_{22R} = (z_{11R} + Z_R)$; subscript 'A' denotes the junction of the plates. $V_A$ and $I_A$ are the mechanical voltage (proportional to stress) and mechanical current (proportional to

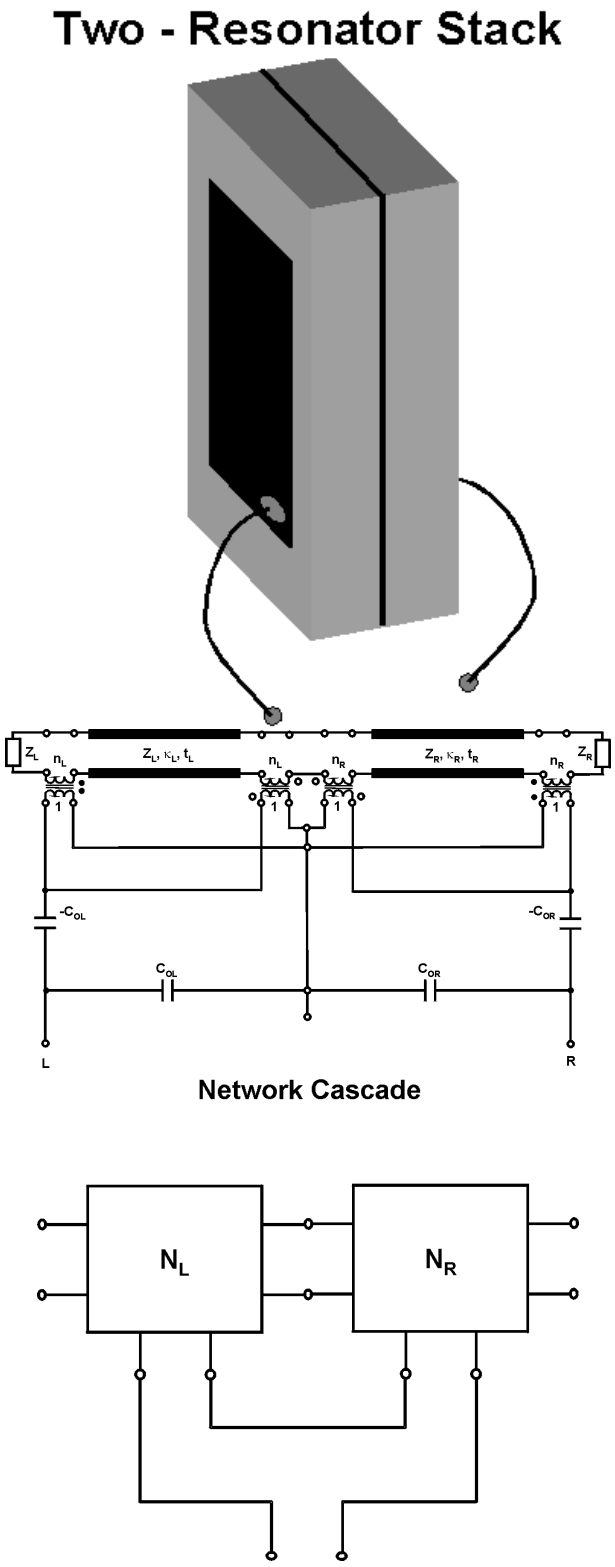


Fig. 2. Two-layer stack and its TL schematic representation. a) Resonator stack. b) Schematic representation of the network model showing the electrical port connections. c) Equivalent circuit consisting of cascade of TLs, including mechanical boundary impedances and electrical port.

particle velocity), respectively, at the interface between the plates. Substitution from the boundary conditions yields

$$0 = \zeta_{11L} I_L + z_{12L} I_A + z_{13L} I \tag{1}$$
$$V_A = z_{12L} I_L + z_{11L} I_A + z_{13L} I \tag{2}$$
$$V_{3L} = z_{13L} I_L + z_{13L} I_A + z_{33L} I \tag{3}$$

$$V_A = z_{11R}(-I_A) + z_{12R} I_R + z_{13R} I \tag{4}$$
$$0 = z_{12R}(-I_A) + \zeta_{22R} I_R + z_{13R} I \tag{5}$$
$$V_{3R} = z_{13R}(-I_A) + z_{13R} I_R + z_{33R} I. \tag{6}$$

Add (3) and (6), and put it first; subtract (4) from (2), and put it second. (This eliminates the common mechanical port voltage $V_A$.) Put (1) third and (5) last. Then, with $[V] = \{V, 0, 0, 0\}^t$ and $[I] = \{I, I_A, I_L, I_R\}^t$, one gets $[V] = [z][I]$. The resulting total impedance matrix, [z], is symmetric and equals

$$\begin{bmatrix} V \\ 0 \\ 0 \\ 0 \end{bmatrix} = \begin{bmatrix} (z_{33L} + z_{33R}) & (z_{13L} - z_{13R}) & z_{13L} & z_{13R} \\ (z_{13L} - z_{13R}) & (z_{11L} - z_{11R}) & z_{12L} & -z_{12R} \\ z_{13L} & z_{12L} & \zeta_{11L} & 0 \\ z_{13R} & -z_{12R} & 0 & \zeta_{22R} \end{bmatrix} \begin{bmatrix} I \\ I_A \\ I_L \\ I_R \end{bmatrix}.$$

The admittance matrix, [y], is the inverse of [z]. Because of the rearrangement of the elements of the composite [z] for the two-plate stack, matrix elements $y_{q1}$ are pertinent. The electrical input admittance $Y_{in}$ is $y_{11}$; $y_{21}$ is proportional to the mechanical displacement at the junction of the two plates; $y_{31}$ and $y_{41}$ are proportional, respectively, to the mechanical displacements at the left and right surfaces (at the electrodes). In general, all elements of [y] are complex. The extension to multilayer stacks, with resulting matrices up to six layers, is given in Appendix B, along with the dual case of excitation by lateral fields [i.e., so-called lateral excitation (LE)].

## IV. Simulations of RAINBOW Structures [30]–[32]

RAINBOW structures are produced by subjecting one surface of a lead-containing planar ceramic to a reducing ambient at high temperatures. After a suitable time, which determines the reduced (cermet) layer thickness, the sample is returned to room temperature. The thermoelastic coefficients of the original ceramic and of the reduced cermet are found to differ substantially. Elissalde *et al.* [30] quote $\alpha = 10$ ppm/K for the cermet phase and $\alpha = 5$ ppm/K for the ceramic. These are typical numbers [31]. During the cooling phase, the cermet portion shrinks faster than the ceramic, producing a warped structure with the cermet layer on the concave side. The combination of domed geometry and internal stresses within the unreduced ceramic layer provide RAINBOW with unique operational characteristics [2], [3]. Although ceramics are relatively well characterized in their physical properties, the cermet layers produced by chemical reduction in the processing of RAIN-

BOW are insufficiently studied to date. Pertinent areas requiring additional future study include the gamut of processing variables; cermet spatial uniformity and isotropy; width of the ceramic/cermet transition region; cermet electrical conductivity, elastic constants, acoustic loss, mass density, and dimensional changes. Because of the absence of adequate experimental data in the literature, a number of assumptions regarding the cermet properties utilized in the simulations have been made. These are briefly given in Appendix C, which also contains remarks pertinent to the material coefficients of the ceramic and the resulting input data used in the simulations.

The departure of the RAINBOW from a planar geometry will be neglected. This is permissible provided that the two principal radii of lateral curvature are much larger than the nominal acoustic wavelength. In plates, this wavelength at the fundamental thickness resonance is about twice the total thickness. For our purposes, sufficiently accurate results are obtained even when the curvatures are only moderately larger than the plate thickness. In addition, the plate lateral extent must, of course, be much greater than its thickness; in practice, ratios exceeding 25 are usually found to be sufficient for the one dimensional, simple thickness mode approximation to yield answers sufficiently accurate for most engineering applications. We also neglect the stress dependencies of the piezoelectric coefficients although these and other effects (e.g., nonlinear elastic constants or radial stress gradients) could be treated parametrically in the mathematics of the network representations provided their dependencies were accurately known. To begin to enable even more accurate simulations, nonlinear finite element methods are being used to model the stress profiles of these structures [9].

### *A. Lumped Mass Approximation Versus Two-Layer Stack*

The lumped-mass approximation is the simplest and most primitive. It consists of modeling a RAINBOW ceramic plate by replacing the reduced (cermet) layer with an equal mass lumped at the surface of the remaining ceramic. The treatment follows that in Section II. The acoustic propagation time within the cermet layer is thus neglected, and one can expect adequate answers only when the reduced layer is but a small fraction of the total plate thickness. The limit of validity of the lumped approximation is determined by comparison with the more realistic case of a two-layer stack, wherein one layer is ceramic, and the other is cermet, and where each occupies a complementary fraction of the total plate thickness. Here, an abrupt ceramic-cermet transition is assumed, and the treatment follows that in Section III. This comparison is given subsequently for various ceramic thicknesses.

Table I gives the computed frequencies for the fundamental harmonic of a single plate with lumped cermet mass, with and without 100-nm silver electrodes placed on the major surfaces. The frequencies listed are $f_R$, the resonance frequency (lower zero reactance point); $f_\varphi$, the frequency of maximum phase; and $f_A$, the antiresonance frequency (upper zero reactance point). It is observed that $f_\varphi$ is approximately the arithmetic average of $f_R$ and $f_A$. All absolute frequencies are in MHz; the results can be rescaled using the nominal fundamental frequency of the unelectroded ceramic, $f_o = v/(2t) = 2.163066$ MHz and the total stack thickness of 1 mm. Simulation results are carried out to six places for the purpose of accommodating various comparisons. In practice, unless measurements are made under laboratory conditions, particularly including temperature control, such frequency stability is very often hard to obtain with current piezoceramic resonators. Table II lists the critical frequencies for a two-layer stack with abrupt ceramic/cermet transition, at the fundamental harmonic, as a function of decreasing ceramic thickness. It is observed that the $f_R$ values monotonically increase, and the $f_A$ values at first increase, then decrease, finally equaling the corresponding $f_R$ values and becoming complex. The $f_\varphi$ values are again approximately the arithmetic means of $f_R$ and $f_A$; they remain real and measurable. The effect of lumped electrode mass is to shift the frequencies downward; the amount varies somewhat with the other variables. The lumped model (Table I) and the two-layer stack (Table II) approach common frequencies in the limit of vanishing cermet. The zeroth-order lumped model departs significantly from the more realistic results of the two-layer stack as the cermet fraction increases.

Normalized frequency difference, often associated with 'bandwidth' in transducer applications, may be defined as $(f_A - f_R)/f_\varphi$. This, in turn, is approximately equal to $1/2r$, where r is the effective capacitance ratio of an equivalent four-element BVD network, provided that $Q \gg r$. From Table I or Table II, for small values of the cermet thickness, $(f_A - f_R)/f_\varphi \approx 11\%$, so that the effective electromechanical coupling factor in either instance is $k_{eff} = (\pi/2)/\sqrt{(2r)} \approx 52\%$, in rough agreement with the coupling factor of the ceramic used; see Appendix C.

The appearance of complex roots seen in Table II arises primarily from the cermet losses. These are of two types, frictional losses characterized by the usual mechanical Q, and a combination of ohmic and dielectric losses described by an electrical Q. In the usual BVD circuit, the mechanical Q is defined as $Q_1$ (mechanical) $= \sqrt{(L_1C_1)/R_1}$, but the electrical Q is undefined. A more refined lumped circuit model is the five-element BVD, with shunt resistor $R_o$ used to model the effects of dielectric and ohmic losses [33]. $R_o$ appears in parallel with the static capacitor $C_o$. With the addition of $R_o$, the electrical Q is defined as $Q_o$ (electrical) $= R_oC_o/\sqrt{(L_1C_1)}$. Because ohmic conductivity and dielectric loss are included in our model, it is appropriate to consider the possible effect of $Q_o$ on the critical frequencies. An examination of the network response at very low frequencies shows, however, that $Q_o \gg Q_1$, and the influence of $Q_o$ is negligible for all entries in Table II. It is thus the mechanical Q that is lowered, with increasing cermet fraction, to the point at which the resonator fails to become inductive. This occurs when $Q_1/r$ falls below approximately 2. As this ratio is approached, the 'band-

TABLE I

CRITICAL FUNDAMENTAL FREQUENCIES, IN MHZ, FOR A SINGLE PLATE AS A FUNCTION OF CERMET FRACTION, WHICH IS CONSIDERED AS A CONCENTRATED MASS LUMPED ON ONE SURFACE. THE INFLUENCE OF LUMPED ELECTRODE MASS IS ALSO GIVEN. THE TOTAL STACK THICKNESS IS 1 MM.

| $t_{ceramic}$ (mm) | $f_R$ | $f_\varphi$ | $f_A$ | $f_R$ | $f_\varphi$ | $f_A$ |
|---|---|---|---|---|---|---|
| | Surface electrodes present | | | Surface electrodes absent | | |
| 1.0 | 1.939934 | 2.051472 | 2.162476 | 1.940515 | 2.052058 | 2.163066 |
| 0.9 | 1.953614 | 2.072188 | 2.190319 | 1.954174 | 2.072761 | 2.190904 |
| 0.8 | 2.001727 | 2.124865 | 2.247580 | 2.002273 | 2.125424 | 2.248153 |
| 0.7 | 2.100617 | 2.229316 | 2.357559 | 2.101180 | 2.229891 | 2.358145 |
| 0.6 | 2.269147 | 2.406802 | 2.543937 | 2.269777 | 2.407441 | 2.544584 |
| 0.5 | 2.540066 | 2.692462 | 2.844245 | 2.540842 | 2.693246 | 2.845036 |
| 0.4 | 2.980660 | 3.157619 | 3.333828 | 2.981740 | 3.158707 | 3.334922 |
| 0.3 | 3.750779 | 3.971366 | 4.190978 | 3.752551 | 3.973146 | 4.192765 |
| 0.2 | 5.333338 | 5.644420 | 5.954082 | 5.337119 | 5.648221 | 5.957898 |
| 0.1 | 10.145431 | 10.733174 | 11.318167 | 10.160103 | 10.747939 | 11.333011 |

TABLE II

CRITICAL FUNDAMENTAL FREQUENCIES, IN MHZ, FOR A TWO-LAYER STACK WITH ABRUPT CERAMIC/CERMET TRANSITION AS A FUNCTION OF CERMET FRACTION. THE INFLUENCE OF LUMPED ELECTRODE MASS IS ALSO GIVEN.

| $t_{ceramic}$ (mm) | $f_R$ | $f_\varphi$ | $f_A$ | $f_R$ | $f_\varphi$ | $f_A$ |
|---|---|---|---|---|---|---|
| | Surface electrodes present | | | Surface electrodes absent | | |
| 0.999 | 1.939966 | 2.051600 | 2.162701 | 1.940547 | 2.052186 | 2.163291 |
| 0.99 | 1.940313 | 2.052780 | 2.164723 | 1.940893 | 2.053365 | 2.165314 |
| 0.9 | 1.948759 | 2.065860 | 2.183652 | 1.949335 | 2.066453 | 2.184260 |
| 0.8 | 1.966015 | 2.077598 | 2.196183 | 1.966596 | 2.078207 | 2.196811 |
| 0.7 | 1.987496 | 2.083851 | 2.192869 | 1.988090 | 2.084469 | 2.193510 |
| 0.6 | 2.009468 | 2.085578 | 2.173001 | 2.010074 | 2.086199 | 2.173637 |
| 0.5 | 2.029473 | 2.083428 | 2.143739 | 2.030086 | 2.084043 | 2.144360 |
| 0.4 | 2.047120 | 2.080158 | 2.115566 | 2.047738 | 2.080768 | 2.116171 |
| 0.3 | 2.063980 | 2.080292 | 2.097149 | 2.064600 | 2.080901 | 2.097749 |
| 0.2 | 2.082410 | 2.087842 | 2.093333 | 2.083035 | 2.088454 | 2.093940 |
| 0.1 | ** | 2.104341 | ** | ** | 2.104971 | ** |

** Frequencies are complex.

TABLE III

CRITICAL FUNDAMENTAL FREQUENCIES, IN MHZ, FOR RESONATOR STACKS CONSISTING OF ONE TO SIX PLATES. PLATES ARE OF EQUAL THICKNESS AND HAVE AVERAGED COMPOSITIONS TO APPROXIMATE A LINEAR MATERIAL GRADIENT ALONG THE THICKNESS COORDINATE.

| Plates | $f_R$ | $f_\varphi$ | $f_A$ | $f_R$ | $f_\varphi$ | $f_A$ |
|---|---|---|---|---|---|---|
| | Surface electrodes present | | | Surface electrodes absent | | |
| 1 | 2.022210 | 2.050585 | 2.078950 | 2.022808 | 2.051183 | 2.079548 |
| 2 | 2.040041 | 2.067253 | 2.095222 | 2.040643 | 2.067843 | 2.095826 |
| 3 | 2.035063 | 2.062664 | 2.090764 | 2.035660 | 2.063253 | 2.091363 |
| 4 | 2.033722 | 2.061473 | 2.089668 | 2.034318 | 2.062140 | 2.090266 |
| 5 | 2.033145 | 2.060968 | 2.089211 | 2.033741 | 2.061557 | 2.089809 |
| 6 | 2.032842 | 2.060704 | 2.088975 | 2.033437 | 2.061293 | 2.089572 |

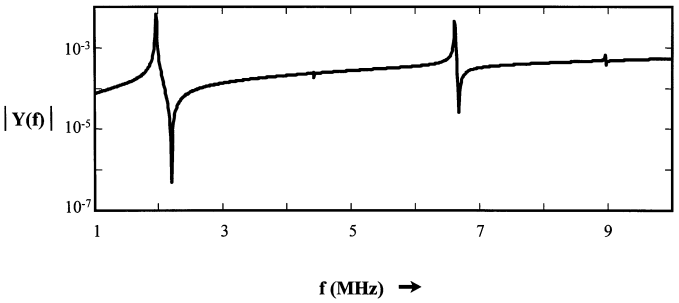


Fig. 3. Mode spectrograph of input admittance magnitude in an extended frequency range for a single plate with lumped mass representing the cermet layer. Ceramic thickness is 0.90 mm; electrode mass is neglected. Resonances, including the even harmonics resulting from the plate asymmetry, are reasonably well predicted in frequency, but absolute admittance levels are somewhat low compared with the more realistic model whose behavior is plotted in Fig. 4.

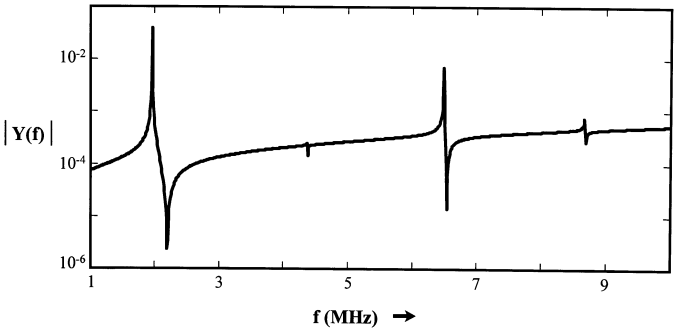


Fig. 4. Extended range mode spectrograph of input admittance magnitude for a two-layer ceramic/cermet stack with abrupt transition. Ceramic thickness is 0.90 mm; electrode mass is neglected. Both the usual odd-harmonic resonances and the additional resonances associated with even harmonic numbers, arising from asymmetry [34], are well predicted in frequency and in absolute admittance level.

width' ceases to be determined by r exclusively and is a function jointly of both r and $Q_1$. A simple method of determining $Q_1/r$ is given subsequently.

In Fig. 3 is plotted a mode spectrograph of input admittance magnitude, in an extended frequency range, for a single plate with lumped mass representing the cermet layer. Ceramic thickness is 0.9 mm; electrode mass is neglected. Because of the asymmetry, both odd and even harmonics are represented [34]. Resonances are reasonably well predicted in frequency, but absolute admittance levels are somewhat low compared with the more realistic two-layer model whose behavior is plotted in Fig. 4. The extended range mode spectrograph of Fig. 4 shows input admittance magnitude for a two-layer stack with abrupt ceramic/cermet transition. Ceramic thickness is 0.9 mm; electrode mass is neglected. Both the usual odd-harmonic resonances and the additional resonances associated with even harmonic numbers arising from asymmetry are well predicted in frequency and in absolute admittance level. As the cermet fraction diminishes, the resonator asymmetry lessens, the even harmonics become sharper and weaker, and they approach an integer relation to the antiresonance of the fundamental.

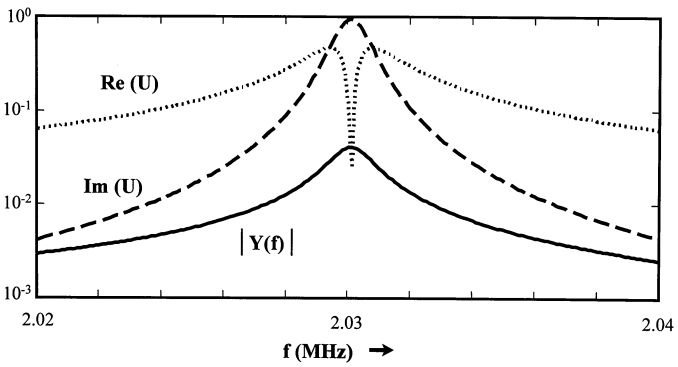


Fig. 5. Magnitude plots of real and imaginary components of displacement at the ceramic (left) surface and of input admittance for a two-layer ceramic/cermet stack with abrupt transition. Frequency range is confined to the vicinity of the resonance frequency. Ceramic thickness is 0.50 mm; electrode mass is neglected. Displacements are in units of 1000s of angstroms per volt.

For the stack plotted in Fig. 4, the resonance at $f_\varphi$ = 2.066453 MHz has a value of $Q_1/r = Q/r = 1638$ and has, therefore, a strong response; the next response, at $f_\varphi$ = 4.359416 MHz, corresponds to the second harmonic and has a value of $Q/r = 1.01$, so that it does not become inductive. The third harmonic, with critical frequencies $f_R$ = 6.471568 MHz, $f_\varphi$ = 6.495574 MHz, and $f_A$ = 6.519902 MHz, has a value of $Q/r = 25.1$ and achieves an inductive region with a reasonably strong response. The fourth harmonic, at $f_\varphi$ = 8.660099 MHz, has a value of $Q/r = 1.46$ so that it, similar to the second harmonic, does not become inductive. In the absence of electrode mass, and for small loss, the antiresonance frequencies should approach integers; because the second and fourth responses do not possess real $f_A$ values, use of $f_\varphi$ may be substituted in these cases to obtain an approximate check. It is found that $[(f_\varphi)_{2nd}/(f_A)_{fund}] \sim 1.996$; similar values are observed for the others.

Fig. 5 shows magnitude plots of the real and imaginary components of displacement at the ceramic ('left') surface and of input admittance for a two-layer stack with abrupt ceramic/cermet transition. Frequency range is confined to the vicinity of the resonance frequency. Plate thicknesses are 0.5 mm, and electrode mass is neglected. Displacements are in units of 1000s of angstroms per volt. One sees, as expected, a phase reversal in the real part of the displacement, which is proportional to the imaginary component of particle velocity, when passing through resonance. All curves monotonically decrease to both sides of plot until other resonances appear at higher frequencies.

### *B. Reduction of a Two-Layer Stack to the Simple BVD Circuit Form*

It was found previously that $Q_o \gg Q_1$, so the simple four-element BVD circuit may be used as a rough indication of input immittance behavior of the stack in a narrow frequency region about resonance. One simple method by which to extract the BVD equivalent is to use the com-

TABLE IV
PARTICLE DISPLACEMENTS, IN ANGSTROMS PER VOLT, FOR A SINGLE RESONATOR. REAL AND IMAGINARY COMPONENTS AND ABSOLUTE MAGNITUDES ARE GIVEN AT THE LEFT (CERAMIC) AND RIGHT (CERMET) SURFACES AT THE THREE CRITICAL FREQUENCIES.

| | L | R |
|---|---|---|
| $f_R$ | | |
| Re(u) | −4.5942 | +4.5942 |
| Im(u) | +372.368 | −372.368 |
| \|U\| | 372.3962 | 372.3962 |
| $f_\varphi$ | | |
| Re(u) | −9.6670 | +9.6670 |
| Im(u) | +0.2578 | −0.2578 |
| \|U\| | 9.6705 | 9.6705 |
| $f_A$ | | |
| Re(u) | −4.7721 | +4.7721 |
| Im(u) | +0.0645 | −0.0645 |
| \|U\| | 4.7726 | 4.7726 |

TABLE V
PARTICLE DISPLACEMENTS, IN ANGSTROMS PER VOLT, FOR A TWO-LAYER STACK. REAL AND IMAGINARY COMPONENTS AND ABSOLUTE MAGNITUDES ARE GIVEN AT THE LEFT (CERAMIC) AND RIGHT (CERMET) SURFACES AND AT THE PLATE JUNCTION FOR EACH OF THE THREE CRITICAL FREQUENCIES.

| | L | A | R |
|---|---|---|---|
| $f_R$ | | | |
| Re(u) | −4.9243 | −0.1098 | +5.3403 |
| Im(u) | +362.489 | −4.6639 | −371.3520 |
| \|U\| | 362.5225 | 4.6652 | 371.3904 |
| $f_\varphi$ | | | |
| Re(u) | −9.7799 | +0.0283 | +10.2170 |
| Im(u) | +0.2794 | −0.0058 | −0.2833 |
| \|U\| | 9.7839 | 0.0289 | 10.2209 |
| $f_A$ | | | |
| Re(u) | −4.7123 | −0.0376 | +5.0270 |
| Im(u) | +0.0689 | −0.0020 | −0.0690 |
| \|U\| | 4.7128 | 0.0377 | 5.0275 |

TABLE VI
PARTICLE DISPLACEMENTS, IN ANGSTROMS PER VOLT, FOR A THREE-LAYER STACK. REAL AND IMAGINARY COMPONENTS AND ABSOLUTE MAGNITUDES ARE GIVEN AT THE LEFT (CERAMIC) AND RIGHT (CERMET) SURFACES AND AT THE PLATE JUNCTIONS FOR EACH OF THE THREE CRITICAL FREQUENCIES.

| | L | A | B | R |
|---|---|---|---|---|
| $f_R$ | | | | |
| Re(u) | −4.5508 | −2.3939 | +2.4248 | +4.9524 |
| Im(u) | +368.366 | +176.359 | −192.574 | −375.185 |
| \|U\| | 368.3937 | 176.3755 | 192.5893 | 375.2173 |
| $f_\varphi$ | | | | |
| Re(u) | −9.6897 | −4.7989 | +5.1222 | +10.0898 |
| Im(u) | +0.2702 | +0.1278 | −0.1416 | −0.2724 |
| \|U\| | 9.6935 | 4.8006 | 5.1242 | 10.0935 |
| $f_A$ | | | | |
| Re(u) | −4.6866 | −2.4044 | +2.5068 | +4.9955 |
| Im(u) | +0.0672 | +0.0313 | −0.0353 | −0.0669 |
| \|U\| | 4.6871 | 2.4046 | 2.5070 | 4.9959 |

puted input capacitance curve of the resonator stack; this is found from the input admittance as $C_{in} = \mathrm{Im}(Y_{in})/\omega$. For the BVD circuit, $C_{in}$ is obtained from the normalized input capacitance relation

$$\left(\frac{C_{in}}{C_o} - 1\right) = \frac{\dfrac{(1-\Omega^2)}{r}}{(1-Q^2)^2 + \left(\dfrac{\Omega}{Q}\right)^2}$$

where the definitions $\Omega = (\omega/\omega_1) = f/f_1$, $r = C_o/C_1$, $Q = Q_1 = \sqrt{(L_1/C_1)}/R_1$, and $\omega_1^2 L_1 C_1 = 1$ have been used. Then, Q/r is found from the extrema of the stack input capacitance curve using, with the assumption $(2Q)^2 \gg 1$,

$$\frac{Q}{r} = \frac{(C_{in})_{max} - (C_{in})_{min}}{C_o}.$$

The capacitance ratio, r, follows from

$$\frac{1}{r} = (1-\Omega^2)\left[\frac{C_{in}}{C_o} - 1\right].$$

In this last relation, $\Omega$ and the corresponding values of $C_{in}$ for the stack are confined to the nearly hyperbolic region of normal dispersion, viz., somewhat away from the region between the extrema of $C_{in}$. As a check, at the extrema, $\Omega^2 = 1 \pm 1/Q$. Knowing the static capacitance, $C_o$ of the stack and its nominal resonance frequency, $f_1$, yields $C_1$, $L_1$, and $R_1$. Applying this method to the fundamental mode of the abrupt ceramic/cermet transition, two-equal-layer stack with negligible electrode mass gives $C_o = 15.8$ pF, $f_1 = 2.030$ MHz, $Q = 1526$, $r = 7.30$, $C_1 = 2.16$ pF, $L_1 = 2.84$ mH, and $R_1 = 23.7$ ohm. One may easily represent the effect of electrodes by the addition of an inductor, $L_e$, in series with $L_1$, as described in [25]. To determine the effective piezoelectric coupling factor from the capacitance ratio requires that it be reduced by unity because we posited a BVD circuit without a negative $C_o$, yet we are exciting the stack by a thickness-directed electric field [25]. Therefore, $r_{TE} = r - 1 = 6.30$ and $k_{eff} = (\pi/2)/\sqrt{(2r_{TE})} \approx 44.3\%$.

### *C. Linear Gradation Approximated by Stacks of Varying Numbers of Layers*

In this second set of simulations, a linear gradient in material constants is successively approximated by using a sequence of layers. Surprisingly few layers are needed to model the convergence of the critical frequencies and motional displacements toward limit points.

Input data are as follows, and the values of the composition of each layer are computed from the averaging relation

$$(1-F)\cdot M_{ceramic} + F \cdot M_{cermet}$$

where M is $\rho$, $1/\sigma$, $\tau_1$, e, or $c^E$. The fraction F is $F = n/2N$ with N equal to the number of layers, and $n =$

TABLE VII

PARTICLE DISPLACEMENTS, IN ANGSTROMS PER VOLT, FOR A FOUR-LAYER STACK. REAL AND IMAGINARY COMPONENTS AND ABSOLUTE MAGNITUDES ARE GIVEN AT THE LEFT (CERAMIC) AND RIGHT (CERMET) SURFACES AND AT THE PLATE JUNCTIONS FOR EACH OF THE THREE CRITICAL FREQUENCIES.

| | L | A | B | C | R |
|---|---|---|---|---|---|
| $f_R$ | | | | | |
| Re(u) | −4.5347 | −3.2955 | −0.0125 | +3.4638 | +4.9364 |
| Im(u) | +370.258 | +252.959 | −9.0272 | −269.964 | −376.459 |
| \|U\| | 370.2859 | 252.9804 | 9.0272 | 269.9866 | 376.4917 |
| $f_\varphi$ | | | | | |
| Re(u) | −9.6638 | −6.7625 | +0.1635 | +7.1759 | +10.0546 |
| Im(u) | +0.2676 | +0.1817 | −0.0080 | −0.1943 | −0.2692 |
| \|U\| | 9.6675 | 6.7649 | 0.1637 | 7.1785 | 10.0582 |
| $f_A$ | | | | | |
| Re(u) | −4.6771 | −3.3562 | +0.0413 | +3.5407 | +4.9859 |
| Im(u) | +0.0666 | +0.0449 | −0.0024 | −0.0481 | −0.0662 |
| \|U\| | 4.6776 | 3.3565 | 0.0414 | 3.5410 | 4.9863 |

TABLE VIII

PARTICLE DISPLACEMENTS, IN ANGSTROMS PER VOLT, FOR A FIVE-LAYER STACK. REAL AND IMAGINARY COMPONENTS AND ABSOLUTE MAGNITUDES ARE GIVEN AT THE LEFT (CERAMIC) AND RIGHT (CERMET) SURFACES AND AT THE PLATE JUNCTIONS FOR EACH OF THE THREE CRITICAL FREQUENCIES.

| | L | A | B | C | D | R |
|---|---|---|---|---|---|---|
| $f_R$ | | | | | | |
| Re(u) | −4.4330 | −3.6546 | −1.4389 | +1.4639 | +3.8939 | +4.8334 |
| Im(u) | +371.122 | +291.423 | +105.026 | −123.824 | −307.835 | −377.046 |
| \|U\| | 371.1487 | 291.4463 | 105.0357 | 123.8331 | 307.8591 | 377.0768 |
| $f_\varphi$ | | | | | | |
| Re(u) | −9.6521 | −7.7271 | −2.8619 | +3.2313 | +8.1734 | +10.0390 |
| Im(u) | +0.2664 | +0.2084 | +0.0738 | −0.0896 | −0.2195 | −0.2678 |
| \|U\| | 9.6558 | 7.7299 | 2.8629 | 3.2325 | 8.1763 | 10.0426 |
| $f_A$ | | | | | | |
| Re(u) | −4.6727 | −3.8175 | −1.4536 | +1.5698 | +4.0441 | +4.9816 |
| Im(u) | +0.0664 | +0.0517 | +0.0180 | −0.0225 | −0.0543 | −0.0659 |
| \|U\| | 4.6732 | 3.8179 | 1.4537 | 1.5700 | 4.0445 | 4.9820 |

TABLE IX

PARTICLE DISPLACEMENTS, IN ANGSTROMS PER VOLT, FOR A SIX-LAYER STACK. REAL AND IMAGINARY COMPONENTS AND ABSOLUTE MAGNITUDES ARE GIVEN AT THE LEFT (CERAMIC) AND RIGHT (CERMET) SURFACES AND AT THE PLATE JUNCTIONS FOR EACH OF THE THREE CRITICAL FREQUENCIES.

| | L | A | B | C | D | E | R |
|---|---|---|---|---|---|---|---|
| $f_R$ | | | | | | | |
| Re(u) | −4.5436 | −3.9846 | −2.3503 | +0.0034 | +2.4472 | +4.2733 | +4.9460 |
| Im(u) | +371.584 | +313.386 | +175.793 | −9.6825 | −194.647 | −328.924 | −377.359 |
| \|U\| | 371.6117 | 313.4114 | 175.8086 | 9.6825 | 194.6620 | 328.9518 | 377.3909 |
| $f_\varphi$ | | | | | | | |
| Re(u) | −9.6460 | −8.2691 | −4.7164 | +0.1835 | +5.1221 | +8.7272 | +10.0307 |
| Im(u) | +0.2657 | +0.2236 | +0.1243 | −0.0083 | −0.1392 | −0.2334 | −0.2671 |
| \|U\| | 9.6497 | 8.2721 | 4.7180 | 0.1837 | 5.1240 | 8.7303 | 10.0343 |
| $f_A$ | | | | | | | |
| Re(u) | −4.6703 | −4.0731 | −2.3632 | +0.0532 | +2.5159 | +4.3239 | +4.9792 |
| Im(u) | +0.0662 | +0.0556 | +0.0306 | −0.0024 | −0.0347 | −0.0577 | −0.0658 |
| \|U\| | 4.6708 | 4.0734 | 2.3634 | 0.0533 | 2.5161 | 4.3243 | 4.9796 |

$1, 3, 5, \ldots (2N-1)$. The value $n = 1$ labels the least reduced layer and is assigned, in the network formalism, to the 'left' plate. Values of $M_{ceramic}$ and $M_{cermet}$ used are found in Appendix C. Arithmetic averaging of material properties to approximate a linear gradient can be replaced by other schemes; for example, harmonic averaging is applied here to the electrical conductivities and, in [29], to elastic stiffnesses. Total stack thickness is 1 mm. All plates are assumed to be of equal thickness (each $1/N^{th}$ of 1 mm). This assumption is again made in the absence of adequate data relating the final thicknesses of ceramic/cermet hybrids to the initial thickness of the ceramic portions from which they were partially reduced. When available, more accurate experimental data may be incorporated simply into the network model. Electrodes are assumed to consist of a 100-nm thickness of silver.

Table III shows the convergence of the critical frequencies to limit points, e.g., approximately 2.0880 MHz in the case of the electroded antiresonance, $f_A$. The case of a single plate is anomalous in that a single plate cannot be asymmetric. It is seen that as few as three plates suffice to obtain frequencies accurate to 0.2%, and six give an accuracy better than 0.05%. The corresponding particle displacements at the stack surfaces and at the plate junctions are given in Tables IV through IX for stacks with different numbers of plates. These are obtained simply in the network model from the currents in the pertinent ports. In a lossless network, the currents are in phase quadrature with the voltage. The presence of loss renders the currents complex. The real parts of the currents are in phase with the driving voltage and are proportional to the real components of the particle velocities and, therefore, to the imaginary components of the displacements and vice versa.

Tables IV through IX list the particle displacements in angstroms per volt for stacks consisting of one to six layers, respectively. Real (reactive) and imaginary (lossy) components and absolute magnitudes are given at the left (ceramic) and right (cermet) surfaces and at the plate junctions for each of the three critical frequencies. It is seen that very few layers are needed to approximate the displacements along the thickness coordinate with reasonable accuracy. Comparing surface amplitudes at $f_R$, which is very nearly the point of maximum displacement, the values for two plates through six plates agree within 2.5%; between four and six plates, the agreement is within 0.1%. For frequencies $f_\varphi$ and $f_A$, where the amplitude levels fall off considerably, the agreement is comparable. Appendix D provides relations for obtaining the displacements within a given plate, if the displacements at its boundaries are known, so that one may interpolate if necessary.

## V. Conclusions

A network realization is given of the one-dimensional vibrations of a stack of piezoelectric plates driven by thickness excitation. Provision is made for inclusion of three separate types of material loss mechanisms in each plate: viscous and dielectric loss and ohmic conductivity. The network model is applied to the characterization of functionally gradient structures. The number of discrete plates that can be accommodated by the network model is not limited, but when applied to functional grading, the number of circuits required to yield good modeling accuracy is shown to be relatively few. Explicit forms of the overall electromechanical network impedance matrix are given for stacks consisting of one to six layers from which the rule of formation for the general case is obtained.

The formalism is used in two sets of simulations. In the first, a ceramic/cermet composite resonator (e.g., a RAINBOW ceramic actuator), considered both as a two-layer asymmetric stack and as a single ceramic plate with asymmetric lumped cermet mass, is simulated and the differing results compared. In the second set, a linear spatial gradient from pure ceramic to pure cermet is approximated using a sequence of stacks of varying numbers. The results are shown to converge rapidly with number, in both frequency and displacement amplitude, with the conclusion that the network formalism can yield practically significant results without undue complication.

In the majority of actuator/sensor/transducer/MEMS applications, the piezoelectric device is embedded in the using circuitry. Therefore, it is highly advantageous to have a characterization of the structure, which is itself a network, and this is the thrust of the developments of this paper. The inclusion of various loss mechanisms in a consistent manner allows the prediction of practical device characteristics such as displacement amplitude, impedance level, and insertion loss.

## Appendix A
## Symbols, Units, and Dimensions.

| | |
|---|---|
| **Material coefficients** | |
| Dielectric permittivity, $\varepsilon$ | farad/meter = F/m = C/(m-V) |
| lossy, $\varepsilon^*$ | |
| Elastic stiffness, c | Pa = $N/m^2$ = $J/m^3$ |
| piezoelectrically stiffened, $\bar{c}$ | |
| lossy, $c^*$ | |
| Mass density, $\rho$ | $kg/m^3$ |
| Ohmic conductivity, $\sigma$ | siemens/meter = S/m |
| Piezo constant, e; d | $C/m^2$ = N/(m−V); C/N = m/V |
| Poisson's ratio, $\nu$ | dimensionless |
| Thermoelastic coefficient, $\alpha$ | $K^{-1}$ |
| ("thermal expansion") | |
| Viscosity, $\eta$ | Pa-s |
| Young's modulus, Y | Pa = $N/m^2$ = $J/m^3$ |
| **Geometry** | |
| Electrode area | $m^2$ |
| A | |
| Plate thickness | meter |
| t = 2h | |
| Thickness coordinate | meter |
| x | |
| **Frequency** | |
| Antiresonance frequency | Hz |
| $f_A$ (upper zero reactance point) | |
| Frequency variable | hertz = Hz = $s^{-1}$ |
| f, $\omega$ | |
| Fundamental mechanical frequency | Hz |
| $f_o = v/2t$ | |
| Maximum phase frequency | Hz |
| $f_\varphi$ | |
| Normalized frequency variable | dimensionless |
| $X = (\pi/2) \cdot (f/f_o)$ | |
| Resonance frequency | Hz |
| $f_R$ (lower zero reactance point) | |
| Time constant | second = s |
| $\tau_1 = \eta/\bar{c}$ | (motional, dynamic) |
| $\tau_o = (\varepsilon/\sigma)$ | (static) |
| **Network and resonator parameters** | |
| Acoustic impedance | kg/s |
| $Z_o = A \cdot \rho \cdot v$ | |
| Admittance matrix | s/kg for mechanical terms (11, 12, 21, 22 matrix elements), |
| [y], [$y^o$], [$y^2$] | A/N for piezoelectric terms (13, 31, 23, 32 matrix elements), |
| | siemens for electrical terms (33 matrix element) |
| Current | ampere = A |
| I, [I] | |
| Electrical input admittance | siemens |
| $Y_{in}$ | |
| Electrical port impedance sum | ohm |
| $\sum$ | |
| Electrical half-length of TL | dimensionless |
| $\theta$ | |
| Impedance matrix | kg/s for mechanical terms (11, 12, 21, 22 matrix elements), |
| [$z^o$], [$z^1$], [$z^2$], [z] | N/A for piezoelectric terms (13, 31, 23, and 32 matrix elements), |
| | ohm for electrical terms (33 matrix element) |
| Mechanical load admittance | s/kg |
| $Y_L$, $Y_R$ | |

| APPENDIX A (continued) | |
|---|---|
| Mechanical load impedance<br>$Z_L$, $Z_R$ | kg/s |
| Mechanical load impedance matrix<br>$[z_{LOAD}]$ | kg/s |
| Piezoelectrically stiffened acoustic velocity<br>v | m/s |
| Piezoelectric transformer turns ratio | C/m |
| Shunt conductance<br>$G_o = \sigma \cdot A/t$, | siemens |
| Shunt conductivity matrix<br>[G] | siemens |
| Surface displacement<br>U, $U_{real}$, $U_{imag}$ | m/V |
| Three-port electromechanical network<br>N | — |
| Total mechanical admittance<br>$\upsilon$ | s/kg |
| Total mechanical impedance<br>$\zeta$ | kg/s |
| Voltage<br>V, [V] | volt = V |
| Wave amplitude<br>P, Q | m/V |
| Wavenumber<br>$\kappa = (\omega/v) = X/h = \theta/t$ | $m^{-1}$ |
| Electrode | |
| Areal mass<br>$m_e = \rho_e t_e$ | $kg/m^2$ |
| Inductance<br>$L_e$ | henry = H |
| Normalized mass<br>$\mu = m_e/\rho h$ | dimensionless |
| BVD | |
| Capacitance ratio<br>$r = C_o/C_1$ | dimensionless |
| Electromechanical coupling factor<br>$k = (\pi/2)/\sqrt{(2r)}$ | dimensionless |
| Input admittance<br>$Y_{in}$ | siemens = S |
| Input capacitance<br>$C_{in} = Im(Y_{in})/\omega$ | F |
| Motional capacitance<br>$C_1$ | F |
| Motional inductance<br>$L_1$ | H |
| Motional resistance<br>$R_1$ | ohm |
| Normalized frequency<br>$\Omega = \omega/\omega_1 = f/f_1$ | dimensionless |
| Quality factor<br>$Q_o$ (electrical) = $R_oC_o/\sqrt{(L_1C_1)}$<br>$Q_1$ (mechanical) = $\sqrt{(L_1/C_1)}/R_1$ | dimensionless |
| Series resonance angular frequency<br>$\omega_1 = 2\pi f_1 = 1/\sqrt{(L_1C_1)}$ | Hz |
| Series resonance frequency<br>$f_1$ | Hz |
| Shunt resistance<br>$R_o$ | ohm |
| Static capacitance<br>$C_o = \varepsilon \cdot A/t$ | farad = F |

TABLE B-I
MATRIX FOR SINGLE PLATE, TE.

$$\begin{bmatrix} \sum & 3A & 3A \\ & \zeta 11L & 2A \\ & & \zeta 22R \end{bmatrix}$$

TABLE B-II
MATRIX FOR TWO-LAYER STACK, TE.

$$\begin{bmatrix} \sum & (3A-3B) & 3A & 3B \\ & (1A+1B) & 2A & -2B \\ & & \zeta 11L & 0 \\ & & & \zeta 22R \end{bmatrix}$$

## APPENDIX B
## MATRICES FOR MULTI-LAYER STACKS OF PLATES

It is again assumed that all plates have common electrode area, A. If shear motion is involved, then it is further assumed that the polar axes of all plates are parallel. To arrive at the total impedance matrix [z] for N lossy plates, electrically connected in series, the same sequence of steps is carried out as for the two-plate prototype. One writes out the three equations of the $[z^2]$ matrix, characterizing each plate, and applies the boundary conditions. The 3N equations that result are assembled as follows. The sum of the third member of all sets yields one equation in the applied voltage, V; then, pairs are subtracted to eliminate the $(N-1)$ voltages at the internal mechanical ports. The remaining two equations (containing the $\zeta$ terms) furnish the final equations for a total of $(N+2)$. The resulting $(N+2)$ by $(N+2)$ impedance matrix is denoted [z]. Its inverse is denoted [y].

Given subsequently are the total impedance matrices resulting from mechanical cascades consisting of up to six plates. The thickness excitation driving voltage appears across the series connection of the electrical ports. For the sake of simplifying the notation, we introduce the following conventions. The left and right total mechanical impedances are denoted $\zeta_{11L}$ and $\zeta_{22R}$. The three-port networks are labeled $N_A, N_B, \ldots$, etc. These are each represented by a lossy $3 \times 3$ impedance matrix $[z^2]$ with an additional subscript to denote the layer represented.

The superscript '2' on $[z^2]$ is now dropped, and the two numerical subscripts on its elements contracted to one, so that a total of only two subscripts is required for each element. We make $z_{11} = z_{22} = z_1$, $z_{12} = z_2$, $z_{13} = z_{23} = z_3$, and $z_{33} = z_4$. Now

TABLE B-III
MATRIX FOR THREE-LAYER STACK, TE.

$$\begin{bmatrix} \sum & (3A-3B) & (3B-3C) & 3A & 3C \\ & (1A+1B) & -2B & 2A & 0 \\ & & (1B+1C) & 0 & -2C \\ & & & \zeta 11L & 0 \\ & & & & \zeta 22R \end{bmatrix}$$

TABLE B-IV
MATRIX FOR FOUR-LAYER STACK, TE.

$$\begin{bmatrix} \sum & (3A-3B) & (3B-3C) & (3C-3D) & 3A & 3D \\ & (1A+1B) & -2B & 0 & 2A & 0 \\ & & (1B+1C) & -2C & 0 & 0 \\ & & & (1C+1D) & 0 & -2D \\ & & & & \zeta 11L & 0 \\ & & & & & \zeta 22R \end{bmatrix}$$

TABLE B-V
MATRIX FOR FIVE-LAYER STACK, TE.

$$\begin{bmatrix} \sum & (3A-3B) & (3B-3C) & (3C-3D) & (3D-3E) & 3A & 3E \\ & (1A+1B) & -2B & 0 & 0 & 2A & 0 \\ & & (1B+1C) & -2C & 0 & 0 & 0 \\ & & & (1C+1D) & -2D & 0 & 0 \\ & & & & (1D+1E) & 0 & -2E \\ & & & & & \zeta 11L & 0 \\ & & & & & & \zeta 22R \end{bmatrix}$$

TABLE B-VI
MATRIX FOR SIX-LAYER STACK, TE.

$$\begin{bmatrix} \sum & (3A-3B) & (3B-3C) & (3C-3D) & (3D-3E) & (3E-3F) & 3A & 3F \\ & (1A+1B) & -2B & 0 & 0 & 0 & 2A & 0 \\ & & (1B+1C) & -2C & 0 & 0 & 0 & 0 \\ & & & (1C+1D) & -2D & 0 & 0 & 0 \\ & & & & (1D+1E) & -2E & 0 & 0 \\ & & & & & (1E+1F) & 0 & -2F \\ & & & & & & \zeta 11L & 0 \\ & & & & & & & \zeta 22R \end{bmatrix}$$

$z_{11A}(= Z_{0A}/j\tan(2X_A))$, for example, becomes simply $z_{1A}$. The next simplification is to enter into the subsequent tables only the subscripts for the matrix elements with the understanding that these represent impedances; that is, $z_{11A}(= z_{1A})$, e.g., will be listed merely as '1A' in the matrix element entry. The quantity '$\sum$' stands for the sum of the $z_4$ impedances; if there are five layers, e.g., then $\sum = z_{4A} + z_{4B} + z_{4C} + z_{4D} + z_{4E}$.

The matrices are arranged so that the column vector representing the voltage forcing function has the form $\{V, 0, 0, \ldots, 0\}^t$. The column vector representing the current responses has the form $\{I, I_A, I_B, I_C, \ldots, I_L, I_R\}^t$. That is, the first current is the true electrical current, common to all the electrical ports. This is followed by the mechanical currents (proportional to the particle velocities) at each mechanical junction between adjacent plates, in order, starting from the left-most plate to the right-most plate. Finally, the last two entries are the mechanical currents at the mechanical junction between the left and right boundary impedances and the outer surfaces of the end plates to which they are attached.

The resulting impedance matrices are symmetric, so only the upper diagonal terms are given; the order of the matrix is always the number of layers plus two.

The rules of formation for N plates can be seen from this sequence. The 11-matrix element, denoted $\sum$, is the sum of the electrical port impedances $(z_{33A} + z_{33B} + \cdots + z_{33N})$. The 12, 13, ... entries are differences $(z_{33(k)}) - z_{33(k+1)}$ of adjacent electrical port impedances; except that the last two entries are the first $(z_{33A})$ and last $(z_{33N})$ electrical port impedances. The principal diagonal entries, starting with the 22 entry, are sums $(z_{11(k)} + z_{11(k+1)})$ of adjacent mechanical port impedances; except that the last two main diagonal entries are the mechanically loaded left $(\zeta_{11L} = \zeta_{11A})$ and right $(\zeta_{22R} = \zeta_{22N})$ mechanical port impedances. The negative entries appearing to the right of the principal diagonal terms, in the positions 23, 34, 45, ..., $(N-1)N$, are equal to $-z_{12B}, -z_{12C}, -z_{12D}, \ldots$, except that the two last such entries, those in the last two columns, are zero. Finally, the entry in the second row of the penultimate column is 2A, and the entry in the last column, second-to-last row, is $(-z_{12N})$. All other entries are zero. [By relabeling variables, one can interchange the last two rows and columns, retain the symmetry, and have the $(-z_{12N})$ entry appear on the same diagonal as the other negative elements; this has not been done to keep the $I_L$ and $I_R$ columns in the sequence given.]

The above formalism applies to stacks of piezoelectric plates driven by TE, wherein all plates are connected electrically in series (common current). The formalism applies as well to stacks of piezoelectric plates driven by LE, wherein all plates are connected electrically in parallel (common voltage). For each plate, one starts with the $[y^o]$ matrix, which is appropriate to LE [17], and incorporates the three internal loss mechanisms in the manner described in the text to arrive at $[y^2]$ matrices. With respect to the TE boundary conditions (BCs) discussed earlier, the LE mechanical BCs at the plate junctions are identical; the BCs at the electrical Ports 3, and the BCs at the mechanically loaded end surfaces are duals. The procedure given for the two-plate TE stack yields, mutatis mutandis, the two-plate LE stack admittance matrix, [y], which equals

$$\begin{bmatrix} (y_{33L} + y_{33R}) & (y_{13L} + y_{13R}) & y_{13L} & y_{13R} \\ (y_{13L} + y_{13R}) & (y_{11L} + y_{11R}) & y_{12L} & y_{12R} \\ y_{13L} & y_{12L} & \upsilon_{11L} & 0 \\ y_{13R} & y_{12R} & 0 & \upsilon_{22R} \end{bmatrix}.$$

The total mechanical admittances $\upsilon_{11L}$ and $\upsilon_{22R}$ equal, respectively, $(y_{11L} + Y_L)$ and $(y_{11R} + Y_R)$, where $Y_L$ and $Y_R$ are the mechanical admittances of the boundary loadings at the outer surfaces of the stack, respectively. The absence of negative signs in all elements of [y], for the LE situation, compared with those in the TE case, arises from the lack of complete duality among the BCs in the two cases. The rule for extending the LE case beyond that of two plates follows by a procedure analogous to that sketched previously for the TE case.

## APPENDIX C
## INPUT DATA FOR THE SIMULATIONS

The thickness-stretch mode is used in the simulations for illustration, and, therefore, '33'-subscripted material coefficients are pertinent. Data characterizing the ceramic are derived from those reported in [29]. The listed $c_{33}^E$ value is used, along with values of $e_{33}$ and $\varepsilon_{33}^S$ calculated via the relations

$$e_{31} = d_{31}(c_{11}^E + c_{12}^E) + d_{33}c_{13}^E,$$
$$e_{33} = 2\,d_{31}c_{13}^E + d_{33}c_{33}^E, \text{and}$$
$$\varepsilon_{33}^S = \varepsilon_{33}^T - 2\,e_{31}\,d_{31} + e_{33}\,d_{33}$$

with the exception that $d_{31}$ has been modified. The coefficient $d_{31}$ was changed from $d_{31} = -271\,(10^{-12})$ to $-171\,(10^{-12})$ because the

TABLE C-I
INPUT DATA.

| Quantity | Unit | Ceramic | Cermet |
|---|---|---|---|
| $\rho$ | $10^3$ kg/m$^3$ | 7.70 | 6.90 |
| $\varepsilon_{33}^{S}$ | $10^{-9}$ F/m | 7.54 | 7.54 |
| $k_{33}$ | % | 47.93* | 0 |
| v | m/s | 4326.1* | 4257.1* |
| $\tau_1$ | s | $10^{-11}$ | $10^{-10}$ |
| $\sigma_{33}$ | S/m | $10^{-9}$ | $10^{+6}$ |
| $\bar{c}$ | GPa | 144.1* | $c_{33}^{E} = 125$ |
| $e_{33}$ | C/m$^2$ | 15.8 | 0 |
| $c_{33}^{E}$ | GPa | 111 | 125 |
| $\tau_0$ | s | 7.54* | 7.54 $10^{-15}$* |

*Indicates entry derived from the relations:
$\bar{c} = c_{33}^{E} + e_{33}^2/\varepsilon_{33}^{S}$; $k_{33} = \left|e_{33}\right|\sqrt{\left(\varepsilon_{33}^{S}\bar{c}\right)}$; $v = \sqrt{\left(\bar{c}/\rho\right)}$; $\tau_0 = \left(\varepsilon^{S}/\sigma\right)$.

reported value, taken with the other coefficients, predicts an unphysical coupling coefficient; the modified value brings an overall consistency to the complete set of elastic, piezoelectric, dielectric, and coupling coefficients when compared with values reported in the literature for similar materials. We assume the permittivity to be nondispersive in the frequency range of the simulations.

A mass density value appropriate to the sintered ceramic is used. Acoustic loss is taken to be roughly $10^3$ times that of crystal quartz, and the total effect of DC electrical conductivity shunted by dielectric loss is assumed to be equivalent to that of a moderate insulator.

The cermet is assumed to be isotropic with longitudinal stiffness calculated from the relation

$$c_{33} = \frac{Y \cdot (1-\nu)}{(1-\nu) - 2\nu^2}$$

using elastic data for a reduced PLZT 5.5/53/47 material: $Y = 66.8\,(10^9)$ Pa and $\nu = 0.380$. Dielectric permittivity is taken, for convenience, to be the same as that of the ceramic. This is of no consequence, as it is dominated by electrical conductivity when $\omega\tau_o \ll 1$, which is the situation here. The viscous loss is taken to be 10 times greater than the viscous loss in the ceramic, and the resistivity roughly five times that of lead metal. A nominal value for mass density of reduced PLZT 5.5/53/47 is also used. The thickness of the cermet is assumed for simplicity and in the absence of sufficient experimental data to be equal to the thickness of the ceramic portion from which it was reduced. It is a simple matter to accommodate thickness changes in the model. These choices are reflected in the material values listed in Table C-1.

## APPENDIX D
## DISPLACEMENTS WITHIN AN INDIVIDUAL PLATE

The displacements within each plate in the stack are completely determined by the displacements at the plate's boundaries. This is true for the components $U_{real}$ and $U_{imag}$ separately. Because the displacements satisfy the TL equations, the displacements within plate 'N' are of the form $[P_N \bullet \sin(\kappa_N x_N) + Q_N \bullet \cos(\kappa_N x_N)]$. The amplitudes $P_N$ and $Q_N$ are found from the boundary displacements. The wavenumber, $\kappa_N$, equals $(\omega/v_N) = X_N/h = \theta_N/t$, where $v_N$ is the stiffened velocity, and $\omega$ the radian frequency of interest (often resonance). The thickness coordinate, measured from the plate center, is $x_N$. The plate half-thickness is $h_N$, $-h_N \le x_N \le +h_N$.

Amplitudes $P_N$ and $Q_N$ are found as follows. The network procedure given in the text provides displacements $U_{real(N-1)}$ and $U_{imag(N-1)}$ at the left of plate 'N', as well as displacements $U_{real(N)}$ and $U_{imag(N)}$ at the right of plate 'N'. Consider, for example, $U_{real}$ at both sides of plate 'B'; one then has $U_{realA}$ and $U_{realB}$ as known inputs. At the left surface, where $x_B = -h_B$:

$$U_{realA} = P_{realB} \bullet \sin(-\kappa_B h_B) + Q_{realB} \bullet \cos(\kappa_B h_B),$$

and at the right surface, where $x_B = +h_B$:

$$U_{realB} = P_{realB} \bullet \sin(\kappa_B h_B) + Q_{realB} \bullet \cos(\kappa_B h_B).$$

Therefore,

$$P_{realB} = \frac{U_{realB} - U_{realA}}{2 \cdot \sin(\kappa_B h_B)} \text{ and}$$

$$Q_{realB} = \frac{U_{realB} + U_{realA}}{2 \cdot \cos(\kappa_B h_B)}.$$

So,

$$U_{real}(x_B) = (U_{realB} - U_{realA}) \cdot \frac{\sin(\kappa_B x_B)}{2 \cdot \sin(\kappa_B h_B)} + (U_{realB} + U_{realA}) \cdot \frac{\cos(\kappa_B x_B)}{2 \cdot \cos(\kappa_B h_B)}$$

and similarly for $U_{imag}(x_B)$, etc.

Note in References.[2]

## REFERENCES


[1] F. Capasso, "Band-gap engineering: From physics and materials to new semiconductor devices," *Science*, vol. 235, pp. 172–176, 1987.

[2] G. H. Haertling, "Rainbow ceramics—A new type of ultra-high-displacement actuator," *Amer. Ceramic Soc. Bull.*, vol. 73, no. 1, pp. 93–96, 1994.

[3] G. H. Haertling, "Ferroelectric ceramics: History and technology," *J. Amer. Ceramic Soc.*, vol. 82, no. 4, pp. 797–818, 1999.

[4] I. A. Aksay, "Smart materials systems through mesoscale patterning," in "US Army Research Office MURI on Functionally Gradient Structures," Princeton University, ARO Contract DAAH04-95-1-0102, Jun. 1995–Nov. 1999.

[5] M. Mehregany, "A multidisciplinary research proposal for MEMS-based smart gas turbine engines," in "US Army Research Office MURI on Functionally Gradient Structures," Case Western Reserve University, ARO Contract DAAH04-95-1-0097, Jul. 1995–Nov. 1999.

[6] N. Hagood, "Multidisciplinary research in smart composite structures," in "US Army Research Office MURI on Functionally Gradient Structures," Massachusetts Inst. Technol., ARO Contract DAAH04-95-1-0104, Jun. 1995–Nov. 1999.

[7] G. P. Carman, "Developing innovative mesoscale actuator devices for use in rotorcraft systems," in "US Army Research Office MURI on Functionally Gradient Structures," Univ. California, Los Angeles, CA, ARO Contract DAAH04-95-1-0095, Jun. 1995–Nov. 1999.

[8] J. S. Vartuli, J. H. Prévost, R. K. Prud'homme, and I. A. Aksay, "Finite element simulations of multilayer cellular piezoelectric transducers," in *Proc. Amer. Ceramic Soc. 101st Annu. Mtg. & Expo.*, 1999, p. 71.

[9] P. Laoratanakul, R. W. Schwartz, E. Skaar, W. Nothwang, and B. T. Han, "Modeling and characterization of stress and geometric effects on the performance of rainbow ceramics," in *Proc. Amer. Ceramic Soc. 101st Annu. Mtg. & Expo.*, 1999, p. 96.


[2]Ref. [1] mentions 'compositionally graded semiconductors,' 'graded-gap transistors,' and 'modulation-doped superlattices.' One may consider these as microscale precursors to what are now referred to as 'functionally gradient materials/structures'. In Ref. [2], compositional variations as functions of thickness coordinate can be produced by subjecting one surface of the ceramic to a reducing atmosphere for limited periods of time. This treatment yields the structure known as RAINBOW (reduced and internally biased oxide wafer).

[10] W. F. Shelley, II, S. Wan, and K. J. Bowman, "Layered and functionally graded piezoelectric ceramics," in *Proc. Amer. Ceramic Soc. 101st Annu. Mtg. & Expo.*, 1999, p. 240.
[11] W. E. Windes and E. D. Steffler, "Fabrication of large functionally graded materials," in *Proc. Amer. Ceramic Soc. 101st Annu. Mtg. & Expo.*, 1999, p. 240.
[12] S. Butterworth, "On a null method of testing vibration galvanometers," in *Proc. Phys. Soc.*, vol. 26, pp. 264–273, 1914.
[13] K. S. Van Dyke, "The electric network equivalent of a piezoelectric resonator," in *Phys. Rev.*, vol. 25, no. 6, p. 895, 1925.
[14] K. S. Van Dyke, "The piezo-electric resonator and its equivalent network," in *Proc. IRE*, vol. 16, pp. 742–764, 1928.
[15] W. P. Mason, *Electromechanical Transducers and Wave Filters*, 2nd ed. Van Nostrand, 1948.
[16] D. A. Berlincourt, D. R. Curran, and H. Jaffe, "Piezoelectric and piezomagnetic materials and their function in transducers," in *Physical Acoustics: Principles and Methods*, vol. 1A, W. P. Mason, Ed. Academic Press, 1964, ch. 3, pp. 169–270.
[17] A. Ballato, H. L. Bertoni, and T. Tamir, "Systematic design of stacked-crystal filters by microwave network methods," *IEEE Trans. Microwave Theory Tech.*, vol. MTT-22, no. 1, pp. 14–25, 1974.
[18] A. Ballato and T. Lukaszek, "Distributed network modeling of bulk acoustic waves in crystal plates and stacks," U.S. Army Electronics Command, Fort Monmouth, NJ, Tech. Rep. ECOM-4311, May 1975.
[19] B. A. Auld, *Acoustic Fields and Waves in Solids*, vol. I, 2nd ed. Krieger Publishing Company, 1990.
[20] J. Rosenbaum, *Bulk Acoustic Wave Theory and Devices*. Artech House, 1988.
[21] R. Krimholtz, D. A. Leedom, and G. L. Matthaei, "New equivalent circuits for elementary piezoelectric transducers," *Electron. Lett.*, vol. 6, no. 13, pp. 398–399, 1970.
[22] D. A. Leedom, R. Krimholtz, and G. L. Matthaei, "Equivalent circuits for transducers having arbitrary even- or odd-symmetry piezoelectric excitation," *IEEE Trans. Sonics Ultrason.*, vol. SU-18, no. 3, pp. 128–141, 1971.
[23] R. Krimholtz, "Equivalent circuits for transducers having arbitrary asymmetrical piezoelectric excitation," *IEEE Trans. Sonics Ultrason.*, vol. SU-19, no. 4, pp. 427–436, 1972.
[24] R. J. Kažys, "Equivalent circuit of the non-uniform piezoelectric transducer," *Ultrasonics*, vol. 14, pp. 115–118, 1976.
[25] A. Ballato and J. Ballato, "Accurate electrical measurements of modern ferroelectrics," *Ferroelectrics*, vol. 182, no. 1–4, pp. 29–59, 1996.
[26] M. Onoe and K. Okada, "Analysis of contoured piezoelectric resonators vibrating in thickness-twist modes," in *Proc. 23rd Annu. Freq. Contr. Symp.*, 1969, pp. 26–38.
[27] A. Ballato, "Resonant strain levels in modern ceramic plate actuators," in *Ceramic Transactions*. vol. 100, K. M. Nair and A. S. Bhalla, Eds. Westerville, OH: The American Ceramic Society, 1999, pp. 443–454.
[28] A. Ballato, "Lateral and thickness excitation of obliquely poled ferroelectric ceramic plates," in *Ceramic Transactions*. vol. 106, K. M. Nair and A. S. Bhalla, Eds. Westerville, OH: The American Ceramic Society, 2000, pp. 309–332.
[29] G. Haertling, "RAINBOWs and ferrofilms—Smart materials for hybrid microelectronics," in *Ceramic Transactions*. vol. 68, K. Nair and V. Shukla, Eds. Westerville, OH: The American Ceramic Society, 1996, pp. 71–96.
[30] C. Elissalde and L. E. Cross, "Dynamic characteristics of rainbow ceramics," *J. Amer. Ceram. Soc.*, vol. 78, no. 8, pp. 2233–2236, 1995.
[31] C. Elissalde, L. E. Cross, and C. A. Randall, "Structural-property relations in a reduced and internally biased oxide wafer (RAINBOW) actuator material," *J. Amer. Ceram. Soc.*, vol. 79, no. 8, pp. 2041–2048, 1996.
[32] G. Li, E. Furman, and G. H. Haertling, "Stress-enhanced displacements in PLZT rainbow actuators," *J. Amer. Ceram. Soc.*, vol. 80, no. 6, pp. 1382–1388, 1997.
[33] A. Ballato, "Piezoelectric resonators," in *Design of Crystal and Other Harmonic Oscillators*. New York: John Wiley & Sons, 1983, pp. 66–122; 432–436.
[34] A. Ballato, T. J. Lukaszek, and G. J. Iafrate, "Subtle effects in high-stability quartz resonators," *Ferroelectrics*, vol. 43, no. 1/2, pp. 25–41, 1982.

**John Ballato** (M'97) is an Assistant Professor of Ceramic and Materials Engineering at Clemson University, where he serves as lead investigator in photonic and opto-electronic materials research and Director of the Center for Optical Materials Science and Engineering Technologies (COMSET). Dr. Ballato received the PhD in 1997 from Rutgers University in ceramic and materials engineering where he studied rare-earth-doped glasses and crystals for applications in fiber and planar lasers, amplifiers, and optical isolators, as well as the drawing of optical fibers. He was recipient of the 1997 Norbert J. Kreidl award from the American Ceramic Society and has been twice honored with the Clemson University Board of Trustees Award for Faculty Excellence. Dr. Ballato has authored over 25 technical articles and holds one patent all dealing with the processing and property characterization and simulation of photonic and opto-electronic materials.

**Robert W. Schwartz** (M'98) is an Associate Professor of Ceramic and Materials Engineering at Clemson University. Dr. Schwartz received his BS degree in science education in 1977 and his MS degree in Chemistry in 1981, both from North Carolina State University. He received his PhD degree in ceramic engineering in 1989 from the University of Illinois, Urbana-Champaign, where he studied the crystallization behavior of lead titanate. Prior to Clemson University, Dr. Schwartz was employed by the BFGoodrich Corporation and Sandia National Laboratories. Dr. Schwartz has authored more than 65 technical articles, has written four book chapters, and has edited two books. In addition, he holds one patent. Dr. Schwartz's current interests include stress-biased piezoelectric actuators and transparent conducting electrode materials.

**Arthur Ballato** (S'55–M'59–SM'71–F'81) received the SB degree in electrical engineering from the Massachusetts Institute of Technology, Cambridge, in 1958; the MS degree in EE from Rutgers University, New Brunswick, NJ, in 1962, and the PhD degree in electrophysics from the Polytechnic Institute of Brooklyn, NY, in 1972. He is Chief Scientist of the US Army CECOM Research, Development & Engineering Center, Fort Monmouth, NJ, and is author of over 300 technical articles and book chapters, more than 50 patents, and editor of several books. Dr. Ballato is a member of the American Physical Society, American Ceramic Society, and Sigma Xi. He is a Chartered Engineer and Fellow of the Institution of Electrical Engineers (London) and Fellow of the Acoustical Society of America. He is an IEEE Ultrasonics, Ferroelectrics, and Frequency Control Society AdCom member, and is its Standards Activities Chairman. He was the Society's Distinguished Lecturer on the topic "Frequency and Time Sources" and received its 1992 Achievement Award.